Human Molecular Genetics, 2019, Vol. 28, No. 10 1726–1737

doi: 10.1093/hmg/ddz010
Advance Access Publication Date: 25 January 2019
General Article

GENERAL ARTICLE

The *TFAP2A–IRF6–GRHL3* genetic pathway is conserved in neurulation

Youssef A. Kousa[1,20,21,†], Huiping Zhu[6,‡‡], Walid D. Fakhouri[7], Yunping Lei[6,§], Akira Kinoshita[8], Raeuf R. Roushangar[1,¶], Nicole K. Patel[2,‡], A.J. Agopian[9], Wei Yang[10], Elizabeth J. Leslie[11], Tamara D. Busch[12], Tamer A. Mansour[3,19,22], Xiao Li[13], Arianna L. Smith[3,††], Edward B. Li[14,15], Dhruv B. Sharma[5], Trevor J. Williams[16], Yang Chai[17], Brad A. Amendt[13], Eric C. Liao[14,15], Laura E. Mitchell[9], Alexander G. Bassuk[12], Simon Gregory[18], Allison Ashley-Koch[18], Gary M. Shaw[10], Richard H. Finnell[6,§] and Brian C. Schutte[1,2,3,4,*]

[1]Departments of Biochemistry and Molecular Biology, [2]Microbiology and Molecular Genetics, [3]Genetics PhD Program, [4]Pediatrics and Human Development, [5]Center for Statistical Training & Consulting, Michigan State University, East Lansing, MI 48824, USA, [6]Dell Pediatric Research Institute, Department of Nutritional Sciences, University of Texas at Austin, Austin, TX 78723, USA, [7]Department of Diagnostic & Biomedical Sciences, School of Dentistry, University of Texas Health Science Center at Houston, Houston, TX 77054, USA, [8]Department of Human Genetics, Nagasaki University, Nagasaki, Japan, [9]Human Genetics Center, Division of Epidemiology, Human Genetics and Environmental Sciences, University of Texas School of Public Health, Houston, TX 77030, USA, [10]Department of Pediatrics, Stanford University School of Medicine, Stanford, CA 94305, USA, [11]Department of Human Genetics, Emory University School of Medicine, Atlanta, GA 30322, USA, [12]Departments of Pediatrics, [13]Anatomy and Cell Biology, University of Iowa, Iowa City, IA 52242, USA, [14]Center for Regenerative Medicine, Massachusetts General Hospital, Harvard Medical School, Boston, MA 02114, USA, [15]Harvard Stem Cell Institute, Harvard University, Cambridge, MA 02138, USA, [16]Department of Craniofacial Biology, University of Colorado Denver at Anschutz Medical Campus, Aurora, CO 80045, USA, [17]Center for Craniofacial Molecular Biology, Ostrow School of Dentistry, University of Southern California, Los Angeles, CA 90033, USA, [18]Duke Molecular Physiology Institute, Duke University Medical Center, Durham, NC 27701, USA, [19]Department of Clinical Pathology, School of Medicine, University of Mansoura, Mansoura, Egypt,

[†]Youssef A. Kousa, http://orcid.org/0000-0001-6049-8144
[‡]Nicole K. Patel, http://orcid.org/0000-0003-2967-4167
[‡‡]Asuragen Inc., Austin, TX 78744, USA.
[§]Center for Precision Enviornmental Health, Departments of Molecular & Cellular Biology and Medicine, Baylor College of Medicine, Houston, TX 77030, USA.
[¶]Institute for Quantitative Health Science and Engineering, Michigan State University, East Lansing, MI 48824, USA.
[††]Biology Department, Kenyon College, Gambier, OH 43022, USA.
Received: November 26, 2018. **Revised:** November 26, 2018. **Accepted:** December 31, 2018

[20]Division of Neurology, Childrens National Health System, [21]Center for Neuroscience Research, The Childrens Research Institute, Washington, DC 20010, USA and [22]Department of Population Health and Reproduction, School of Veterinary Medicine, University of California, Davis, CA 95616, USA

*To whom correspondence should be addressed at: Microbiology and Molecular Genetics, Biomedical Physical Sciences Building, Room 5162, 567 Wilson Road, Michigan State University, East Lansing, MI 48824-4320, USA. Tel: 517 884-5346; Fax: (517) 353-8957; Email: schutteb@msu.edu

Abstract

Mutations in *IRF6*, *TFAP2A* and *GRHL3* cause orofacial clefting syndromes in humans. However, *Tfap2a* and *Grhl3* are also required for neurulation in mice. Here, we found that homeostasis of *Irf6* is also required for development of the neural tube and associated structures. Over-expression of *Irf6* caused exencephaly, a rostral neural tube defect, through suppression of *Tfap2a* and *Grhl3* expression. Conversely, loss of *Irf6* function caused a curly tail and coincided with a reduction of *Tfap2a* and *Grhl3* expression in tail tissues. To test whether *Irf6* function in neurulation was conserved, we sequenced samples obtained from human cases of spina bifida and anencephaly. We found two likely disease-causing variants in two samples from patients with spina bifida. Overall, these data suggest that the *Tfap2a-Irf6-Grhl3* genetic pathway is shared by two embryologically distinct morphogenetic events that previously were considered independent during mammalian development. In addition, these data suggest new candidates to delineate the genetic architecture of neural tube defects and new therapeutic targets to prevent this common birth defect.

Introduction

Interferon Regulatory Factor 6 (*IRF6*), Transcription Factor Activation Protein 2A (*TFAP2A*) and Grainy Head-Like 3 (*GRHL3*) encode transcription factors that are required for orofacial development in humans and mice (1–9). Mutations in *IRF6* or *GRHL3* cause Van der Woude syndrome (VWS), an autosomal dominant form of cleft lip and palate that also includes pits in the lower lip (MIM: 119300). Mutations in *TFAP2A* cause branchiooculofacial syndrome, another autosomal dominant orofacial clefting disorder with a phenotype that can include lip pits (MIM: 113620). The overlap of the phenotypes caused by mutations in these three genes is consistent with the hypothesis that *TFAP2A*, *IRF6* and *GRHL3* function in a shared genetic pathway. Genetic and molecular studies support this hypothesis. For example, AP-2A, the protein encoded by *TFAP2A*, transactivates *IRF6* through binding to *MCS9.7* (10), an enhancer element with activity that replicates much of *IRF6* endogenous expression (11–13). Moreover, the derived (non-ancestral) allele of rs642961, a common single nucleotide polymorphism (SNP) located in the *MCS9.7* enhancer, disrupts binding of AP-2A and is strongly associated with cleft lip and palate (12). It is not known why a derived allele has become common in human populations despite harboring risk for a congenital disease. These data suggest that AP2A directly regulates *IRF6* during orofacial development. Furthermore, studies in human keratinocytes and zebrafish showed that IRF6 regulates *GRHL3* expression (14,15), and mutations in *GRHL3* cause a syndrome identical to that of *IRF6* (4). Together, these previous observations suggest that *TFAP2A*, *IRF6* and *GRHL3* comprise a gene regulatory network. This is supported by mouse genetics, where knocking out any of these three genes results in abnormal skin, limb and craniofacial development (1,5–7,16,17). However, mice that lack either *Tfap2a* or *Grhl3* also have neural tube defects (6,7,16). The neural tube defects are located rostrally (exencephaly) and caudally (kinked or curly tail) in both mutant mice, and an open neural tube (lumbosacral spina bifida) is observed in *Ghrl3* mutant mice. Loss of *Grhl3* leads to primary failure of caudal neural tube closure prior to adhesion as a result of neural folds that fail to elevate and remain convex, with defects by E9.5 (16). Similar to GRHL3, loss of TFAP2A results in delayed elevation of neural folds that also remain convex with morphological changes apparent by E9.5 (6,7). In addition, embryos that lack *Tfap2a* have an exceptional body wall defect with thoraco-abdominoschisis. In contrast, neural tube defects are not obvious in mouse embryos that lack *Irf6*. Here we used a loss-of-function and gain-of-function allelic series to study the role of *Irf6* in neural tube morphogenesis. We observed that homeostasis of *Irf6* function is required for neurulation and this function is mediated, in part, through a regulatory network that includes *Tfap2a* and *Grhl3*.

Results

Homeostasis of Irf6 is required for neurulation

To test whether *Irf6* is required for neural tube development, we modulated *Irf6* expression *in vivo* using an allelic series in mice. To reduce *Irf6* expression, we crossed mice that carried a hypomorphic allele ($Irf6^{neo}$) (18) with a null allele ($Irf6^{gt}$) (1), herein referred to as $Irf6^{-}$, and examined embryos at E17.5. Embryos heterozygous for the hypomorphic allele ($Irf6^{neo/+}$; n = 17) appeared grossly normal (Fig. 1B). However, compound heterozygous embryos ($Irf6^{neo/-}$, n = 18) had a completely penetrant curly and shortened tail (Fig. 1A). The skin and limbs of these embryos appeared grossly normal. These data suggest that the tail defect in *Irf6*-deficient mice is not secondary to abnormal skin development.

To study the effect of gain-of-function of *Irf6* in neural tube closure, we used the *KRT14* promoter to over-express *Irf6* ($Tg^{KRT14\text{-}Irf6}$) (19). Surprisingly, while 109 of 126 (86%) transgenic embryos appeared grossly normal (Fig. 1D), we found that 17 (14%) embryos have rostral neural tube defects, including 11 embryos with exencephaly (Fig. 1E) and 6 embryos with anencephaly, split face, thoraco-abdominoschisis and a kinked tail (Fig. 1F and F′). The rostral neural tube defect in mice demonstrates that *Irf6* is required for neurulation.

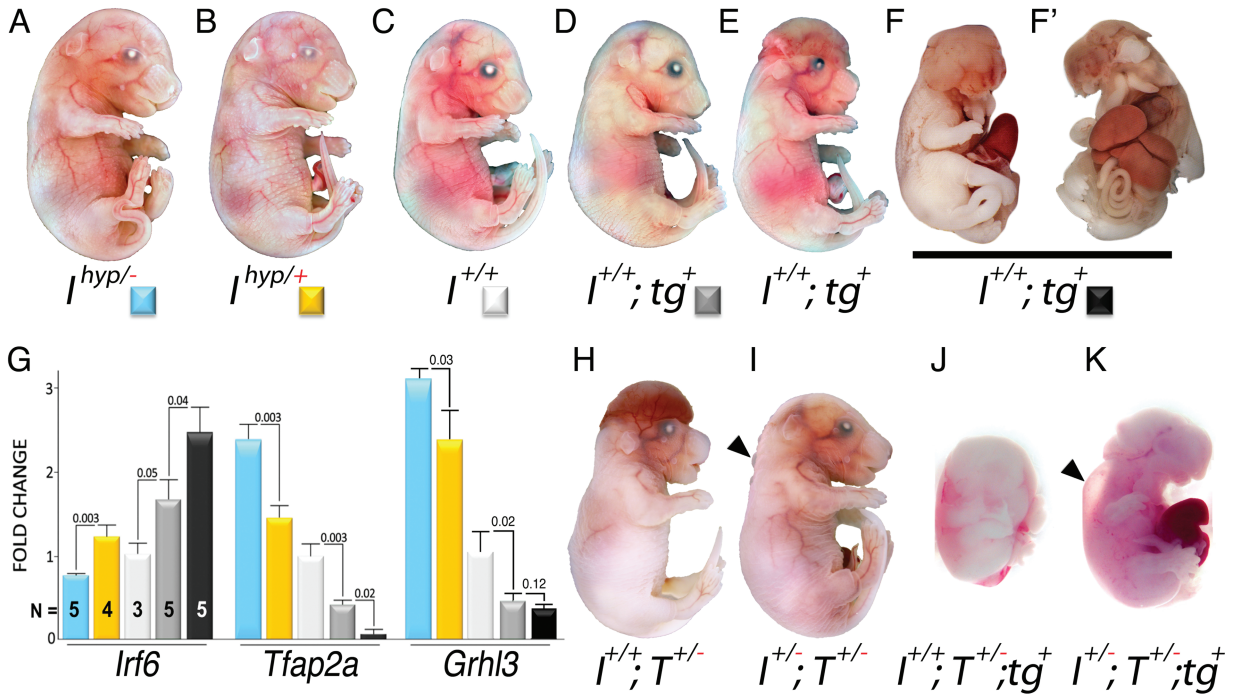

Figure 1. Homeostasis of *Irf6* is required for neurulation. **(A–F′)**, E17.5 embryos from the *Irf6* allelic series, with increasing gene dosage from left to right. Compound heterozygotes for the *Irf6* hypomorphic and null alleles (A) have a completely penetrant kinked tail ($N = 18$). Embryos that are heterozygous for the *Irf6* hypomorphic allele (B) are not grossly different from wild-type embryos (C). Embryos that are wild type at the *Irf6* locus, but carry the *K14-Irf6* transgene, had one of three phenotypes; 86% (109/126) normal (D), 9% (11/126) with exencephaly (E) and 5% (6/126) with anencephaly, thoraco-abdominoschisis and kinked tail (F, lateral and F′, ventral view of same embryo). **(G)** Relative levels of *Irf6*, *Tfap2a* and *Grhl3* mRNA from dorsal back skin from embryos represented in (A–D and F) ($N = 5$, 4, 3, 5 and 5, respectively). Relative level of *Irf6* mRNA is higher in more severely affected embryos that carry the transgene (D versus F), suggesting variable *Irf6* expression from the *K14-Irf6* transgene. Relative level of *Tfap2a* mRNA decreases as *Irf6* mRNA levels increase. Relative level of *Ghrl3* mRNA decreases significantly for each group of embryos except between the embryos that carry the *K14-Irf6* transgene (D versus F). **(H and I)** 10% (7/68) of E17.5 embryos that are singly heterozygous for the *Tfap2a* null allele have exencephaly (H) while 0% (0/69) of embryos that are double heterozygotes for both *Irf6* and *Tfap2a* null alleles have exencephaly (I). **(J and K)** 55% (10/18) of E15.5 embryos that are heterozygous for the *Tfap2a* null allele and carry the *K14-Irf6* transgene have rostral neural tube defects and appear smaller than littermates (J), whereas 9% (1/11) of these embryos that also carry the *Irf6* null allele are less severely affected and had sub-epidermal blebbing (arrowhead; K). Sub-epidermal blebbing was also observed in embryos double heterozygotes for both *Irf6* and *Tfap2a* (arrowhead; I).

The most severely affected $Tg^{KRT14\text{-}Irf6}$ embryos phenocopied *Tfpa2a* knockout embryos (6,7,20). In addition, the $Tg^{KRT14\text{-}Irf6}$ embryos with the intermediate phenotype were similar to embryos that are heterozygous for the *Tfap2a* null allele, which is associated with incompletely penetrant exencephaly (21). We therefore hypothesized that expression of *Irf6* from the transgene varies between embryos and that *Irf6* negatively regulates expression of *Tfap2a*. To test these hypotheses, we measured steady-state levels of *Irf6* and *Tfap2a* mRNA from dorsal skin of E17.5 embryos across the allelic series. As expected, we observed a gradient of steady-state levels of *Irf6* across the allelic series $Irf6^{neo/-} < Irf6^{neo/+} < Irf6^{+/+} < Tg^{KRT14\text{-}Irf6}$ (Fig. 1G). In addition, the level of *Irf6* expression in the $Tg^{KRT14\text{-}Irf6}$ embryos was variable, a phenomenon often observed with transgenes (22), and correlated with the severity of the phenotype. Moreover, we found a dose-dependent negative correlation between *Irf6* and *Tfpa2a* expression, whereby the most severely affected transgenic embryos had the highest amount of *Irf6* and the least amount of *Tfpa2a*. These data are consistent with the hypothesis that Irf6 negatively regulates *Tfap2a* expression and provides a rationale for how embryos that over-express *Irf6* can phenocopy embryos that are deficient for *Tfap2a*. The mechanism for this negative regulation is unknown, as we were unable to detect binding of IRF6 to the ectoderm enhancer for *Tfap2a* (23). However, we did detect binding at the mesodermal enhancer for *Tfap2a* (24) and binding to other known targets, including *Tfap2c*, *Stratifin* and *Grhl3* loci (Supplementary Material, Fig. S1) (14,15).

To confirm that endogenous *Irf6* functions to negatively regulate *Tfap2a*, we tested whether the *Irf6* null allele could rescue the exencephaly in mice that are heterozygous for *Tfap2a*. We found that 10% (7/68) of the single heterozygote $Tfpa2a^{LacZ/+}$ embryos had exencephaly (Fig. 1H). However, none of the 69 double-heterozygous ($Irf6^{+/-};Tfpa2a^{LacZ/+}$) littermates had exencephaly (Fig. 1I; $P = 0.0063$). We conclude that *Irf6* and *Tfpa2a* genetically interact during development of the rostral neural tube and that the mechanism is negative regulation of steady-state levels of *Tfap2a* mRNA by Irf6.

To further validate this genetic interaction, we combined the $Tg^{KRT14\text{-}Irf6}$ transgene with the *Tfap2a* null allele. As expected, embryos that were heterozygous for the *Tfap2a* null allele and carried the $Tg^{KRT14\text{-}Irf6}$ transgene had an increase in the penetrance of anencephaly, split face and thoraco-abdominoschisis from 5% (6/126) to 63% (10/18, $P = 0.0001$). However, one of these embryos also displayed a more severe phenotype than the *Tfap2a* null embryos, with a more dramatic loss of cranial structures and a visibly shorter spinal axis (Fig. 1J). This observation suggested that *Irf6* was interacting with another gene. We tested *Grhl3* because *Irf6* was shown to regulate *Grhl3* expression (14,15) and loss of *Grhl3* causes both rostral and caudal neural tube defects (16). We measured levels of *Grhl3* mRNA from embryos of the allelic series, and as with *Tfap2a*, we observed an inverse

relationship between *Grhl3* and *Irf6* (Fig. 1G). Thus, reduction in levels of both *Tfap2a* and *Grhl3* mRNA may explain the more severe phenotype in embryos that are heterozygous for *Tfap2a* and carry the *K14-Irf6* transgene. To test whether endogenous *Irf6* function could modify the effects of the *K14-Irf6* transgene, we analyzed littermates that were also heterozygous for the *Irf6* null allele. The phenotype of embryos with the *Irf6* null allele ($Irf6^{+/-}$;$Tfap2a^{+/-}$; $Tg^{+/KRT14\text{-}Irf6}$) was less severe (Fig. 1K) and less penetrant (1/11 versus 10/18; $P = 0.01$). Since the null allele at the endogenous *Irf6* locus modified the effects of the *K14-Irf6* transgene, we conclude that the transgene perturbs normal *Irf6* function.

Tfap2a and Grhl3 interact genetically

In the allelic series, loss of *Irf6* function resulted in a tail defect but was not apparent until E17.5. We considered the role of *Irf6* in secondary neurulation and somite development. In formation of the spine, secondary neurulation (formation of the posterior neural tube) uses mechanisms distinct from those of primary neurulation and is complete prior to E14.5 (25). On the other hand, somite development and differentiation leads to formation of critical supporting structures, for example tendons, muscles and vertebra. Isolated vertebral defects are clinically described as spina bifida occulta and have been described in patients with Popliteal Pterygium Syndrome (PPS) (26,27). Importantly, PPS is caused by dominant negative mutations in *IRF6*. We predicted the tail defect in hypomorphic *Irf6* mice resulted from loss of function of *Tfap2a*, *Grhl3* or both. Our rationale was that loss of function of either of these genes causes a tail defect, and even though we observed that *Irf6* negatively regulated expression of these genes in ectoderm, we and others previously observed that *Irf6* can also positively regulate *Grhl3* (14,15).

We measured expression of *Tfap2a* and *Grhl3* mRNA in whole tail tissue from $Irf6^{neo/-}$ embryos at E17.5. We observed a reduction in both *Tfap2a* and *Grhl3* mRNA levels (Fig. 2A). However, the decrease in expression of each gene was less than 2-fold, and therefore the decrease in either gene alone could not be expected to account for the kinked tail in the $Irf6^{neo/-}$ embryos, as mice that are heterozygous for either *Grhl3* or *Tfap2a* do not have a kinked tail (6,7,16). To test whether combined reduction of *Grhl3* and *Tfap2a* expression levels could account for the kinked tail, we crossed mice that are heterozygous for the *Grhl3* and *Tfap2a* null alleles. As expected, none of the 132 single heterozygotes had a curly tail (Fig. 2B and C) but 17 of 119 (14%) $Tfpa2a^{+/-}$;$Grhl3^{+/-}$ double-heterozygous embryos had a curly tail (Fig. 2D) that was also apparent in adulthood (Fig. 2E). These data are highly significant ($P = 0.0001$), suggesting a genetic interaction between *Tfap2a* and *Grhl3* during development of the tail. In addition, these data are consistent with the hypothesis that coordinated positive regulation of *Tfap2a* and *Grhl3* by *Irf6* can explain the tail defects in *Irf6*-deficient embryos. Considering the association of PPS with spina bifida occulta, e.g. vertebral anomalies, and later manifestation of tail defects in $Irf6^{neo/-}$, the most likely site of this interaction is somite development or differentiation.

To explore the genetic interaction between *Tfap2a* and *Grhl3*, we crossed mutant mice to generate embryos with zero, one or two mutant alleles at each locus. In addition to the tail defect shown above, double-heterozygous mice had an incompletely penetrant rostral neural tube defect (Fig. 2J). However, the frequency was not different than expected for *Tfap2a*+/− single heterozygous embryos (9/119). Embryos with two null alleles of *Grhl3* and one for *Tfap2a* (Fig. 2M) had a phenotype similar to the most severely affected *Grhl3* knockout embryos (Fig. 2L), with curly tail, lumbosacral spina bifida and exencephaly. However, the penetrance of exencephaly was higher (14/16 versus 5/16; $P = 0.003$), and the triple mutant embryos appeared smaller than the *Grhl3* knockout littermates. Embryos with two null alleles of *Tfap2a* and one null allele of *Grhl3* (Fig. 2K) were more severely affected than *Tfap2a* knockout embryos (Fig. 2H), with defects in cranial tissues, and the embryos appeared smaller. The double knockout embryos were notable in two ways (Fig. 2N). First, although they were the most severely affected, smallest and most pale, surprisingly, they did not have lumbosacral spina bifida that is characteristic of *Ghrl3* knockout embryos (N = 3; Supplementary Material, Fig. S2), suggesting that not all genetic interactions between *Grhl3* and *Tfap2a* are synergistic. Second, the phenotype of the *Tfap2a* and *Grhl3* double knockout embryos resembled embryos that were heterozygous for the *Tfap2a* null allele and carried the $Tg^{KRT14\text{-}Irf6}$ transgene (Fig. 1J). This observation is consistent with the expression data in skin, where *Irf6* negatively regulates both *Tfap2a* and *Grhl3*, suggesting that the synergistic interactions between *Tfap2a* and *Grhl3* occur primarily in tissues derived from ectoderm.

Irf6 is co-expressed with AP-2a

Loss of *Tfpa2a* leads to pathology as early as E9.5 (6). We predicted that endogenous IRF6 and the IRF6 transgene driven by the *KRT14* promoter would be expressed at or before this timepoint to modify and phenocopy the *Tfap2a* phenotype. At E8.75, we observed strong IRF6 signal in the neural plate, neural folds and non-neural ectoderm with two different antibodies (Fig. 3A and B). Further, we found co-localization of IRF6 and AP-2a in the neural folds and non-neural ectoderm (Fig. 3C; Supplementary Material, Fig. S3). At E9.5, we found that IRF6 was expressed in the neural ectoderm and co-localized with RHOB (Fig. 3E), a marker of migrating neural crest cells (28). However, IRF6 expression appeared to be restricted to early migrating neural crest cells (Fig. 3G). We also observed co-localization of KRT14 with IRF6 in the neural ectoderm and early migrating neural crest cells (Fig. 3H). Finally, we observed co-staining between IRF6 and AP-2a in non-neural ectoderm and early migrating neural crest cells (Fig. 3I). These protein expression data are supported by publicly available gene expression profiles for neural and non-neural ectoderm at E8.5 (Supplementary Table S1). In sum, these data suggest that expression of IRF6 and KRT14 is consistent with the neurulation defects observed in $Tg^{KRT14\text{-}Irf6}$ embryos and those with loss-of-function alleles of the endogenous *Irf6* gene. As further confirmation, we performed immunostaining for IRF6 and RHOB in the $Tg^{KRT14\text{-}Irf6}$ mutant embryos. We observed a robust IRF6 signal in the neural and non-neural ectoderm (Fig. 3F). Moreover, a similarly strong IRF6 signal was detected in early migrating neural crest cells with concomitant loss of the signal for AP-2a (Fig 3I versus J). Together, these data demonstrate that IRF6 from endogenous and transgenic loci cooperate to repress AP-2a expression. Histological staining of wild-type and mutant embryos further suggested an abnormal optic vesicle and a disorganized facial mesenchyme at E9.5 (Fig. 3K versus L).

Tfap2a is required for MCS9.7 activity

MCS9.7 is a critical enhancer for *IRF6* orofacial expression (11,12). To test whether the *MCS9.7* enhancer drives expression of *Irf6*

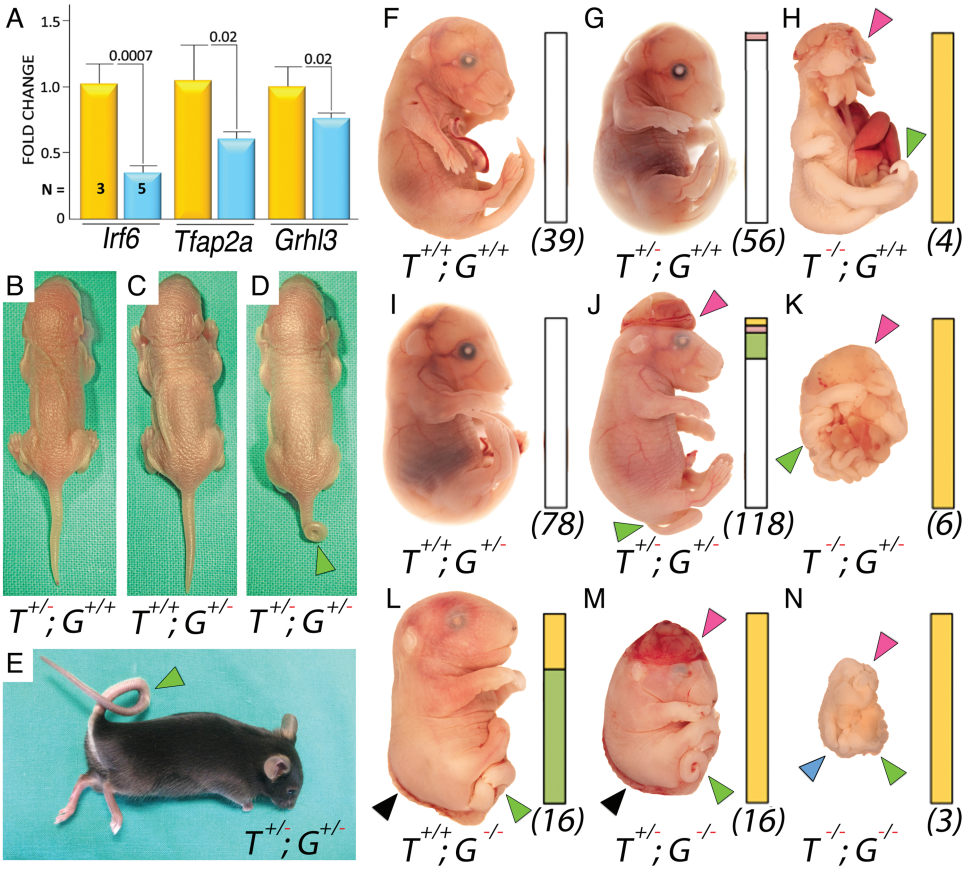

Figure 2. *Tfap2a* and *Grhl3* interact genetically. (**A**) Levels of *Grhl3* and *Tfap2a* mRNA decrease in whole tail tissue when *Irf6* expression level is reduced, in contrast to dorsal skin where their levels increase as *Irf6* gene dosage is decreased. (**B–D**) Tails are normal in mice that are singly heterozygous for either *Tfap2a* (B) or *Grhl3* (C), but a curly tail was observed in mice that are double heterozygotes for *Grhl3* and *Tfap2a* null alleles (D). (**E**) Adult mice that are double heterozygotes for *Grhl3* and *Tfap2a* null alleles have a curly tail and are viable and fertile. (**F–N**), Representative embryos for the indicated genotypes. The three columns represent $Tfap2a^{+/+}$ ($T^{+/+}$), $Tfap2a^{+/-}$ ($T^{+/-}$) and $Tfap2a^{-/-}$ ($T^{-/-}$), respectively. The three rows represent $Grhl3^{+/+}$ ($G^{+/+}$), $Grhl3^{+/-}$ ($G^{+/-}$) and $Grhl3^{-/-}$ ($G^{-/-}$), respectively. Thus, the diagonal shows the embryos that are wild type (F), double heterozygotes (J) and double knockouts (N). Note that embryos with at least three null alleles (K, M and N) appear smaller and paler. Arrows point to neural tube defect (NTD), rostral NTD (red), curly tail (green) and lumbosacral spina bifida (black). Significantly, the double knockout embryos do not have lumbosacral spina bifida (blue arrow). Histogram adjacent to each embryo represents the distribution of phenotypes for each genotype. For example, fraction of embryos with wild-type phenotype (white), caudal NTD (green), rostral NTD (red), both rostral and caudal (yellow). The number of embryos for each genotype (N) is shown below each histogram.

in tissues relevant to the neural tube, we analyzed embryos that carry the *MCS9.7-LacZ* reporter transgene ($Tg^{MCS9.7\text{-}LacZ/+}$; 11). As previously observed, the *MCS9.7* enhancer was active in the hindbrain and somites at E10 (Fig. 4A and B), and sectioning revealed activity in the neuroepithelium of the hindbrain (Fig. 4B′). At E12.5 we observed two stripes of *MCS9.7* activity along the neural tube beginning at the level of the hindbrain and ending just caudal to the hind limb (Fig. 4C–E). Upon sectioning, the two stripes were due to MCS9.7 activity at the junction of the developing non-neural epithelium and the neural tube (Fig. 4E′). We also observed *MCS9.7* activity in the dorsal root ganglion and somites (Fig. 4E and E′). By E14.0, the two stripes had merged into a single faint stripe along the dorsal midline (Fig. 4F). Lateral stripes were also observed along the tail (Fig. 4G and H), and sectioning showed that these stripes originated from connective tissues of the tail, including the four tendons most prominently (Fig. 4H′).

AP-2A regulates *IRF6* by directly binding to *MCS9.7* (10). To test whether *MCS9.7* activity in the tail was dependent on *Tfap2a*, we generated mice that carried the *MCS9.7-LacZ* transgene but lacked *Tfap2a*. We detected no difference in *MCS9.7* activity until E14, when we observed that the continuous lateral stripes along the tail in wild-type embryos (Fig. 4G and H) were discontinuous in the *Tfap2a* mutant embryos (Fig. 4I–K). Sectioning revealed that the *MCS9.7* activity in the tendons of tail in wild-type embryos (Fig. 4H′) was lost in $Tfpa2a^{-/-}$ embryos and tail tissues were disorganized (Fig. 4K′). Thus, while *MCS9.7* is active in neural tube development, its regulation by *Tfap2a* is limited to non-ectodermal tissues. Considering coordinated positive regulation of *Tfap2a* and *Grhl3* by *Irf6* in the tail as described above, this result further suggests that *Tfap2a* has a positive feedback function on the *Irf6* enhancer in somite development. These data further support the role of the IRF6-TFAP2A-GRHL3 axis in mammalian neural tube and spine development.

IRF6 is required in human neurulation

We hypothesized that rare and common DNA variants in *IRF6* confer risk for human neural tube defects. In silico analysis of the 3′UTR of *IRF6* revealed a multiple species conserved sequence we called *MCS21*. *MCS21* contained a predicted binding

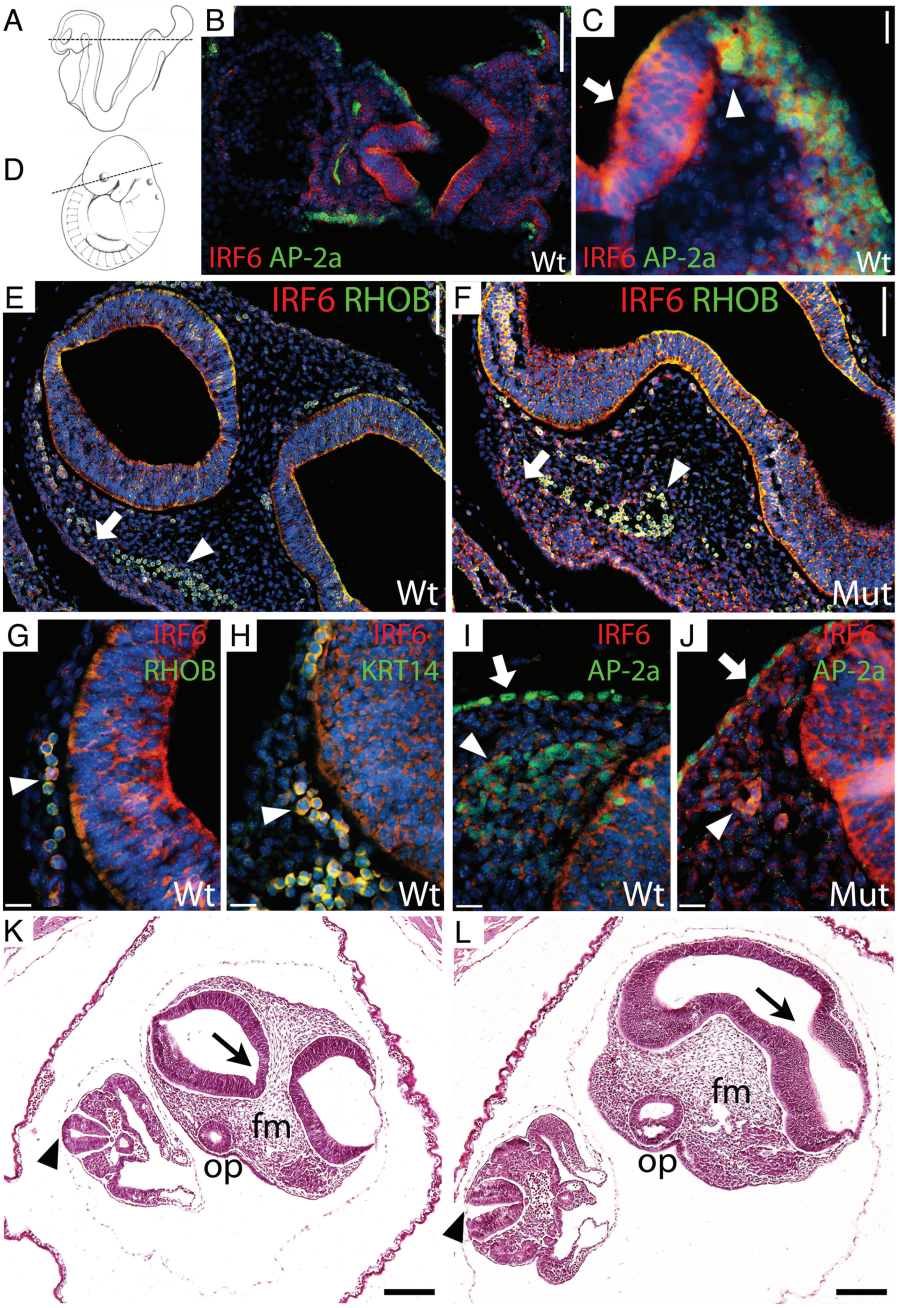

Figure 3. IRF6, KRT14 and AP-2a expression during neurulation. (**A**) Illustration of E8.75 embryo with line indicating plane of section for Fig. 3B and C (A). (**B**) Immunostaining shows IRF6 (red) and AP-2a (green). (**C**) Magnified view of neural plate (arrow) and non-neural ectoderm at E8.75 showing IRF6 (red) co-localization with AP-2a (green) at the neural plate border (arrowhead). DAPI marks the nuclei (blue). (**D**) Illustration of E9.5 embryo with line indicating plane of section for Fig. 3E–L (**D**). (**E–J**) Immunostaining of wild-type (E, G–I) and mutant littermates (F, J). Compared with wild-type embryos (E), mutant littermates (F) have ectopic IRF6 expression (red) (arrow) and abnormal neural crest cell migration (arrowhead). IRF6 (red) and RHOB (green) are co-expressed in neural crest cells (G) (arrowhead). IRF6 (red) is co-expressed with KRT14 (green) in both the neural ectoderm (Supplementary Material, Fig. S2) and early migrating neural crest cells (H) (arrowhead) and with AP-2a (green) in the early migrating neural crest cells (I and J) (arrowhead). Relative to wild-type embryos (I), mutant littermates (J) have ectopic IRF6 expression (red) and loss of AP-2a staining (green) in the neural crest (arrowhead). In contrast, AP-2a expression in the non-neural ectoderm is unaffected (I versus J) (arrow). (G and **H**) Histological analysis of wild-type (**K**) and mutant embryos (**L**). Wild-type embryos have both rostral (arrow) and caudal (arrowhead) neural tube closure, with intact optic vesicle and facial mesenchyme (K). Mutant embryos had abnormal optic vesicles (op) and disorganized facial mesenchyme (fm) (H). Scale bar: B, E, F = 100 µm. Scale bar: C, G–J = 20 µm. Scale bar: K and L = 200 µm.

site for miR-96 and an additional binding site for miR-6767-5p was created by the presence of the derived allele for SNP rs17317411. *MCS21* conferred instability to a reporter mRNA and the derived allele for the SNP further destabilized *IRF6* mRNA (Supplementary Material, Fig. S4) consistent with miRNA regulation. Consequently, mutations that abrogated or enhanced miRNA binding could alter human *IRF6* mRNA leading to rostral neural closure or tail defects as observed in the mouse. Therefore, we sequenced *MCS21* in 133 cases of anencephaly obtained from the Hereditary Basis of Neural Tube Defects study

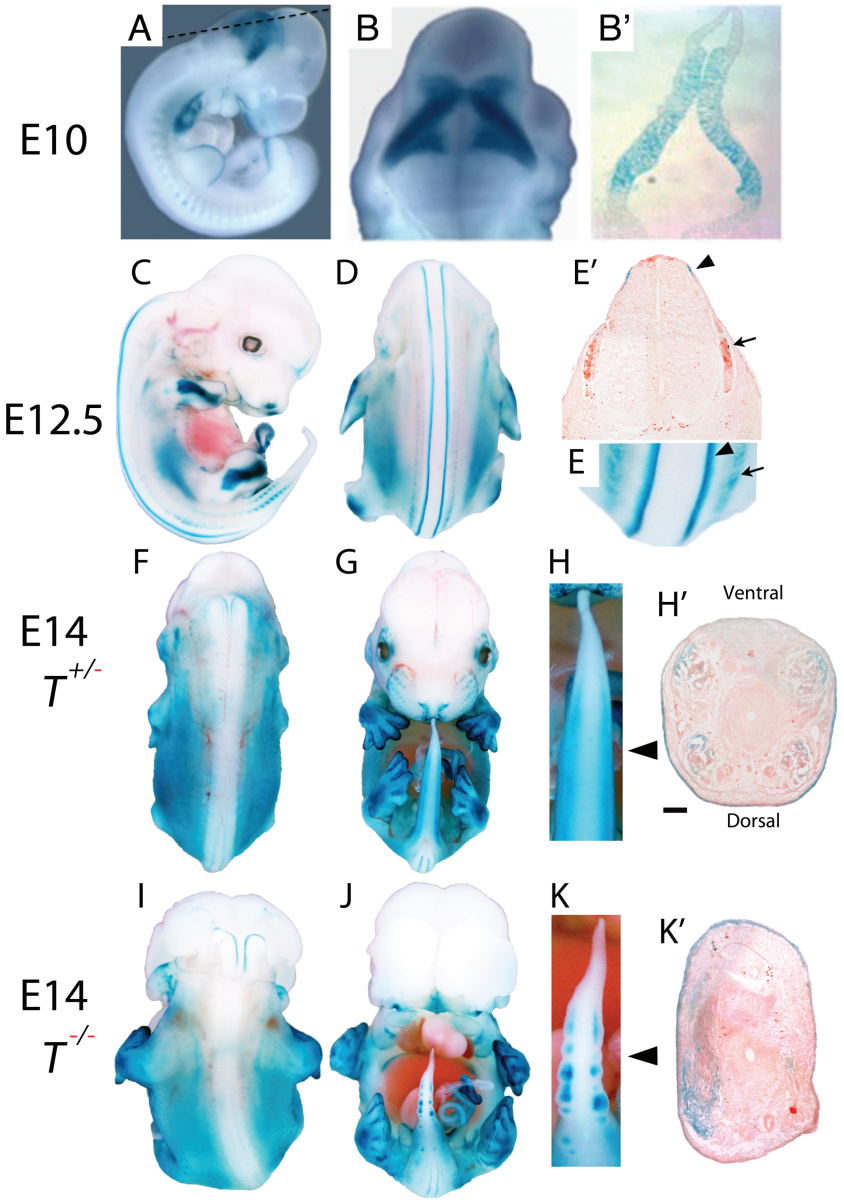

Figure 4. *Tfpa2a* is necessary for *MCS9.7* activity along the posterior spinal cord. (**A–K′**) *In vivo* activity of the *MCS9.7* enhancer is indicated by staining with X-gal (blue) using mice that carry the $Tg^{MCS9.7\text{-}LacZ}$ transgene. (**A and B′**) *MCS9.7* is active at E10 in hindbrain neuro-epithelium. Lateral (A) and dorsal (B) views of a representative whole-mount stained embryo at E10. Coronal section, indicated by the dashed line (A), shows activity in the neuro-epithelium (B′). At E12.5, lateral (**C**) and dorsal (**D and E**) views of whole-mount stained embryos suggest *MCS9.7* activity along the neural plate border (arrowhead) and dorsal root ganglion (arrow) ($N = 3$) and confirmed using a transverse section (E′). At E14, dorsal (**F, H, I and K**) and ventral (**G and J**) views show that *MCS9.7* is active along the tail of wild-type embryos (F–H) ($N = 4$), but has a discontinuous, punctate pattern in *Tfap2a* knockout embryos (I–K) ($N = 7$). Sectioning reveals expression in the epithelium and the four tendons of the tail in wild-type embryos (H′) at the plane of section (H, arrowhead). In contrast, *Tfap2a* knockout embryos have a dysmorphic tail (K) with loss of MCS9.7 activity in both the dorsal epithelium and mesenchymal tail tissue (K′) at the plane of section (K, arrowhead). Scale bar: **H′** and **K′** = 200 µm.

(29), and we sequenced *MCS21*, *MCS9.7* and the *IRF6* protein-coding region in 192 cases of spina bifida from the California Birth Defects Monitoring Program (CBDMP; 30). We observed no new DNA variants in *MCS21*, and none of the common variants were over-represented in the anencephaly cohort (Supplementary Material, Table S2). In the spina bifida cohort, we identified 39 variants (Supplementary Material, Table S3), including c.-3–3 C>A and c.1279 C>T. These two variants were not found in nearly 61 000 exomes (Exome Aggregation Consortium) nor were they found in an independent set of 198 cases of spina bifida (Supplementary Material, Table S4) that were recruited at Children's Memorial Hospital in Chicago, IL (31). The first variant alters a highly conserved C nucleotide at the −3 position of the 3′splice site and is predicted to disrupt splicing of exon 3 (32). The second variant is a non-synonymous substitution in exon 9 that alters a highly conserved amino acid, Asp427Tyr (Fig. 5A and C). Structural analysis showed that Asp427 occurs at the junction of the c-terminal alpha helix of IRF6 (Fig. 5B and D). Prior work on IRF5, the paralog most similar to IRF6 showed that this domain is required for dimerization and transactivation (33). Using a recently reported *in vivo* zebrafish assay (34), Asp427Tyr (D427Y) variant failed to rescue embryos

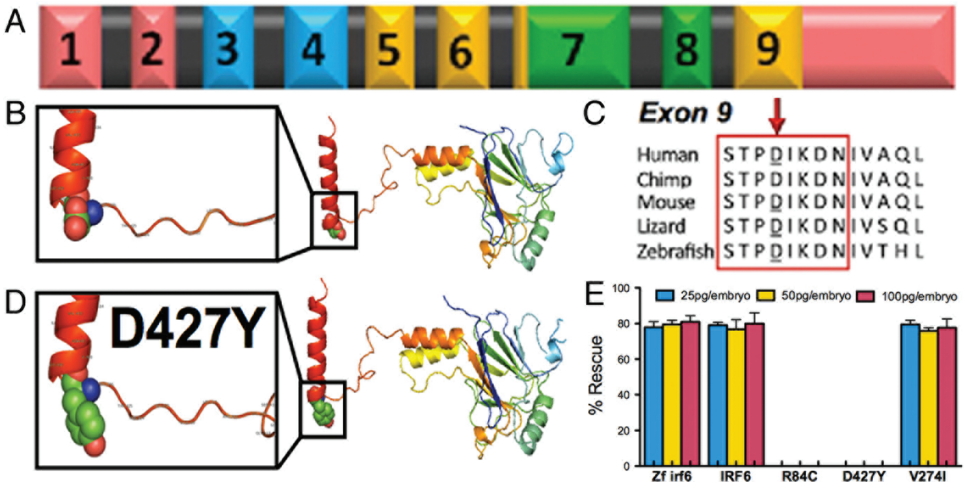

Figure 5. A missense mutation identified in a patient with spina bifida. Genomic structure for *IRF6* **(A)**. Exons 1 and 2 contain the 5′UTR (red). Exons 3 and 4 encode the DNA binding domain (blue). Exons 7 and 8 encode the protein binding domain (green). Exon 9 encodes the predicted auto-inhibitory domain (yellow) and the 3′UTR (red). Predicted protein structure of IRF6 **(B)**. The aspartic acid residue at 427 is highly conserved in vertebrates **(C)**. Based on the predicted protein structure of IRF6 **(B)**, this amino acid is located at the base of the C-terminal helix of IRF6. This ribbon structure is based on the crystal structures of IRF5. Sequencing in individuals with spina bifida identified a rare variant, D427Y **(D)**. *In vivo* analysis of this variant using a zebrafish model showed that D427Y, like R84C, did not rescue our zebrafish model at various concentrations of 25, 50 and 100 picograms of mRNA per embryo. V274I did rescue our zebrafish model. Zebrafish and human IRF6 are provided as baseline. Percent shown is the number of rescued embryos at 24 h post-fertilization, relative to the number of injected embryos. Three biological replicates were performed for reach concentration and variant tested. Errors bars represent standard error of the mean.

that lacked IRF6 (Fig. 5E). This finding was very similar to R84C (Fig. 5), a well-recognized mutation that can lead to both VWS and PPS (2,35) and in contrast to V274I, a benign variant (36). Surprisingly, we previously reported Asp427Tyr as a likely disease-causing mutation in a patient with VWS (37). Likewise, a recent study identified a mutation in *GRHL3* in a patient with spina bifida (38), and that same mutation had previously been found in a patient with VWS (4). These observations are consistent with the previously suggested hypothesis that DNA variants in the same gene, and even the same variant, can lead to orofacial clefting or spina bifida, depending on the genetic background and/or environmental exposures of the individual (38).

To test for an association between common variants of *IRF6* and neural tube defects, we performed case/control analysis with 425 cases and 447 matched controls from the CBDMP (30). Cases were diagnosed with myelomeningocele, a severe form of spina bifida. We also performed association studies on two family-based cohorts, a 500 case/parent trio population from the HBNTD study (29) and a 284 case/parent trio population recruited by researchers from the University of Texas-Houston (39). In these three populations, we focused on three variants; rs642961 in *MCS9.7* that impacts AP-2a binding, rs17371411 in *MCS21* that altered mRNA stability and rs76145088. The latter SNP is also located in *MCS9.7*, and the derived allele is predicted to abrogate binding to a highly conserved site for the TEAD/TEF family of transcription factors (40). These factors mediate Hippo signaling and are essential for neural tube development (41,42). The derived allele for each of these SNPs arose on different haplotypes (Supplementary Material, Table S6). In these populations (Supplementary Material, Tables S7–S11), the only significant signal we detected was between rs17317411 and cases of lipomyelomeningocele ($N = 50$; $P = 0.04$; Supplementary Material, Table S10), a form of spina bifida where failure of the neural tube closure induces surrounding mesenchymal cells to differentiate into adipose tissue (43). While we did not find strong statistical evidence that common variants contribute risk for neural tube defects in humans, the finding of two likely disease-causing alleles in *IRF6* in cases of spina bifida suggests that its function in neurulation is conserved.

Discussion

We found that *Tfap2a*, *Irf6* and *Grhl3* are components of a gene regulatory network required for neurulation. Since this network is also required for formation of the lip, palate, limbs and epidermis, which develop at different times and places during embryogenesis, we suggest that the *Tfap2a-Irf6-Grhl3* network is a fundamental pathway for multiple morphogenetic processes. In addition, several lines of evidence suggest that the primary role for this network is to regulate ectodermal development. First, while the expression of these genes is not limited to ectoderm (44–46), they are co-expressed in tissues derived from ectoderm throughout development. Second, *Irf6* over-expression, which led to a rostral neural tube defect, was driven in this study by the promoter for *Keratin 14*. Third, the type and severity of the neurulation defects were significantly associated with the level of *Irf6* expression measured in stratified skin at E17.5. While skin is a heterogeneous tissue, previous expression analysis showed that AP-2a, IRF6 and GRHL3 are all primarily expressed in the ectodermally derived keratinocytes of the epidermis (1,16,47). However, the pleiotropic effects in the mutant embryos suggest additional potential roles in mesoderm and endoderm development. In support of this hypothesis, the curly tail in the *Grhl3* mutant embryos was previously shown to be due to expression and function in hindgut endoderm (45). Furthermore, established cellular pathways suggest that both GRHL3 and AP-2a are required for neural fold elevation and adhesion, with apparent defects by E9.5 (6,7,16). Similarly, histological analysis suggests that over-expression of IRF6

results in delay of caudal neural tube closure prior to adhesion at E9.5. Furthermore, we found that reducing *IRF6* expression results in tail abnormalities most likely resulting from defects in somite development or differentiation. Sub-epidermal blebbing in double heterozygotes for both *Irf6* and *Tfap2a*, irrespective of the $Tg^{KRT14\text{-}Irf6}$ (Fig. 1I and K), suggests that PDGFRA and PI3K-AKT signaling is downstream of these transcription factors (48,49).

To date, the only known murine models displaying both anencephaly and a thoraco-abdominoschisis are *Tfpa2a* knockout embryos and those that over-express *Irf6* in ectoderm. However, *Palladin* and *Grhl2* knockout embryos also display anencephaly and abdominoschisis but have an intact thoracic wall. Considering the morphological similarity, future work should address whether these genes are part of the same pathway as *Irf6* and *Tfpa2a*, although prior work suggested that *Tfpa2a* did not interact with *Grhl2* (50). Similarly, mice that lacked *Chuk* (51), *14–3-3σ* (5), *Ripk4* (52) or *Kdf1* (53) produced embryos that phenocopy the *Irf6* knockout. Considering the shortened abnormal tail in *Irf6* knockout embryos, future work may uncover analogous roles for these genes. Consistent with this hypothesis, mice lacking both *Chuk* and *Ikbkb* (*Ikk2*) have exencephaly (54). Moreover, mutations in *CHUK* can cause Cocoon Syndrome (MIM: 600664), an autosomal recessive lethal disorder with major malformations including rostral neural tube defects (55). Taken together, morphogenesis has gained a new unifying pathway from which candidate genes may be tested in cases of human birth defects (56). This is significant because, while overall infant morbidity and mortality have decreased with the 'health transition', the incidence of birth defects remains stubbornly high, accounting for an ever greater portion of infant morbidity and mortality (57).

Materials and Methods

Ethics statement

All animal use protocols and procedures were approved by the Institutional Animal Care and Use Committees at Michigan State University. Use of samples from the CBDMP was approved by the State of California Health and Welfare Agency Committee for the Protection of Human Subjects. Use of samples from the HBNTD was approved by the Internal Review Board (IRB) at Duke University Medical Center. Use of samples at the University of Iowa and the University of Texas School of Public Health were approved by their respective IRBs.

Morphological, histological and molecular analyses of murine tissue

All mouse strains used in this study were published previously. *Irf6 KO* (1), *Grhl3 KO* (58) and the $Irf6^{neo}$ hypomorphic (18) alleles and the $Tg^{+/KRT14\text{-}Irf6}$ (19) transgene were on a C57Bl/6 background. *Tfap2a KO* (7) *and* $Tfap2a^{LacZ}$ (20) alleles were on a Black Swiss background. For timed matings, the presence of a copulation plug is denoted as E0.5. Genotyping was performed as described previously (1). All crosses had expected genotype distributions (Supplementary Material, Table S12–S20). Gross morphological, histological and molecular assessments were performed as described previously (11). Antibodies used were the following: Irf6 (Sigma-Aldrich, SAB2102995, St. Louis, MO and Schutte Lab, SPEA, East Lansing, MI), AP-2a (3B5, sc-12726, Santa Cruz, CA), Keratin 14 (Novocastra, NCL-L-LL002, Buffalo Grove, IL), RhoB (56.4H7, University of Iowa Hybridoma Facility), goat anti-mouse and goat anti-rabbit (Molecular Probes, Applied Molecular Probes, Boyds, MD). Nuclei were labeled with DAPI (Invitrogen, Gaithersburg, MD). Imaging was performed as previously described (11).

Quantification of RNA

Total RNA was isolated from the indicated tissues as recommended (TRIzol, Ambion, Waltham, MA). Steady-state levels of mRNA were quantified using SYBR Green as recommended (Applied Biosystems, Beverly, MA) and Polymerase chain reaction (PCR) primers listed in Supplementary Material, Table S21 and as previously published (63,64). We used the cycle threshold (Ct), set within the linear range of amplification, to analyze the data. We obtained the delta-Ct relative to Beta-Actin and the delta–delta Ct and the fold change, relative to wild-type embryo levels for the gene of interest.

Chromatin Immuno-Precipitation

Quantitative polymerase chain reaction and chromatin immunoprecipitation experiments were performed as described previously (59). Experiments to measure mRNA stability were performed as described previously (60).

Human sequencing, genotyping and analysis

Sanger sequencing and mutation analysis were performed as described previously (61). Sequencing primers are in Supplementary Material, Table S22. Samples from 425 cases and 451 matched controls from the CBDMP were genotyped and analyzed as described previously (30). Samples from 500 case/parent trios from the HBNTD were genotyped and analyzed as described previously (29). Samples from 284 case/parent trios from the University of Texas-Houston trios were genotyped on the Infinium HumanExome BeadChip v1.1 (Illumina, San Diego, CA). We excluded samples with >5% missing genotypes or SNVs with >10% missing genotypes. Trios with Mendelian errors for >1% of SNVs or Single-nucleotide polymorphism (SNPs) with Mendelian errors in >1% of individuals were excluded. The analyses were conducted on 284 trios to evaluate the association between the inherited (i.e. case) genotype and NTD risk, using a multinomial likelihood approach implemented using the software EMIM (62).

Statistics

For quantitative Polymerase chain reaction (qPCR), an unpaired, one-tailed Student[1]s *t* test was used to determine significance. Data represent mean ± SEM. For Mendelian ratios, we used Chi-Squared Analysis to determine if the observed and predicated genotype distributions were significantly different. A *P*-value of ≤0.05 was considered significant.

Supplementary Material

Supplementary Material is available at *HMG* online.

Acknowledgements

The authors acknowledge the ongoing legacy of Dr Marcy Speer through the use of samples obtained from the 'Hereditary Basis of Neural Tube Defects' study conducted under her leadership at Duke University Medical Center. The authors also acknowledge Dr Jeffrey C. Murray for providing patient samples and sequencing resources. We thank the California Department of Public Health Maternal Child and Adolescent Health Division for providing data for these analyses. The findings and conclusions in this report are those of the authors and do not necessarily represent the views of the California Department of Public Health.

Conflict of Interest statement. The authors declare no competing financial interests.

Funding

Michigan State University (to B.C.S.); National Institutes of Health (NIH) (DE13513 to B.C.S., F31DE022696 to Y.A.K. and B.C.S., DE025060 to E.J.L.); UT-Health School of Dentistry in Houston (to W.D.F., DE12728 and DE019843 to T.J.W.); and partial funding provided by CDC (5U01DD001033) and NIH (P01HD067244, GM072859 to G.M.S.). The funders had no role in study design, data collection and analysis, decision to publish, or preparation of the manuscript.

Author contributions

Y.A.K., along with B.C.S., conceived of the work. Y.A.K. designed and performed all murine crosses and experiments, performed statistical analyses, prepared the figures and tables, interpreted the data and wrote the manuscript. Y.A.K. also contributed to the design, analysis and interpretation of human sequencing data. A.K. generated the *Irf6*^{neo} hypomorphic allele. W.D.F., X.L. and B.A.A. designed, performed and analyzed *in vitro* experiments. A.L.S., R.R.R. and N.K.P. performed mouse genotyping and statistical analyses. N.K.P. also collected and analyzed quantitative expression data and created the illustration of the murine embryos. T.J.W. and Y.C. contributed critical reagents. D.B.S. contributed to and reviewed the statistical analyses of mouse data. H.Z. contributed to design, analysis and interpretation of human sequencing and genotyping data and performed human sequencing and genotyping along with Y.L. and T.D.B.. T.M., E.J.L., A.J.A., W.Y. and L.E.M. contributed to the analysis of human sequencing data. R.H.F., G.M.S., A.G.B., S.G. and A.A.K. provided DNA samples from human volunteers and supervised and analyzed DNA sequencing and genotyping. Y.A.K., E.B.L., E.C.L. and B.C.S. contributed to the design of *in vivo* testing of D427Y, and E.B.L. and E.C.L. performed and supervised the assay. B.C.S. supervised the project, established and maintained collaborations, interpreted data and revised the manuscript. All authors edited the manuscript.

References

1. Ingraham, C.R., Kinoshita, A., Kondo, S., Yang, B., Sajan, S., Trout, K.J., Malik, M.I., Dunnwald, M., Goudy, S.L. and Lovett, M. (2006) Abnormal skin, limb and craniofacial morphogenesis in mice deficient for interferon regulatory factor 6 (Irf6). *Nat. Genet.*, **38**, 1335–1340.
2. Kondo, S., Schutte, B.C., Richardson, R.J., Bjork, B.C., Knight, A.S., Watanabe, Y., Howard, E., de Lima, R.L., Daack-Hirsch, S., Sander, A. *et al.* (2002) Mutations in IRF6 cause Van der Woude and popliteal pterygium syndromes. *Nat. Genet.*, **32**, 285–289.
3. Milunsky, J.M., Maher, T.A., Zhao, G., Roberts, A.E., Stalker, H.J., Zori, R.T., Burch, M.N., Clemens, M., Mulliken, J.B., Smith, R. *et al.* (2008) TFAP2A mutations result in branchio-oculo-facial syndrome. *Am. J. Hum. Genet.*, **82**, 1171–1177.
4. Peyrard-Janvid, M., Leslie, E.J., Kousa, Y.A., Smith, T.L., Dunnwald, M., Magnusson, M., Lentz, B.A., Unneberg, P., Fransson, I., Koillinen, H.K. *et al.* (2014) Dominant mutations in GRHL3 cause Van der Woude Syndrome and disrupt oral periderm development. *Am. J. Hum. Genet.*, **94**, 23–32.
5. Richardson, R.J., Dixon, J., Malhotra, S., Hardman, M.J., Knowles, L., Boot-Handford, R.P., Shore, P., Whitmarsh, A. and Dixon, M.J. (2006) Irf6 is a key determinant of the keratinocyte proliferation–differentiation switch. *Nat. Genet.*, **38**, 1329–1334.
6. Schorle, H., Meier, P., Buchert, M., Jaenisch, R. and Mitchell, P.J. (1996) Transcription factor AP-2 essential for cranial closure and craniofacial development. *Nature*, **381**, 235–238.
7. Zhang, J., Hagopian-Donaldson, S., Serbedzija, G., Elsemore, J., Plehn-Dujowich, D., McMahon, A.P., Flavell, R.A. and Williams, T. (1996) Neural tube, skeletal and body wall defects in mice lacking transcription factor AP-2. *Nature*, **381**, 238–241.
8. Kousa, Y.A. and Schutte, B.C. (2016) Toward an orofacial gene regulatory network. *Dev. Dyn.*, **245**, 220–232.
9. Kousa, Y.A., Moussa, D. and Schutte, B.C. (2017) IRF6 expression in basal epithelium partially rescues Irf6 knockout mice. *Dev. Dyn.*, **246**, 670–681.
10. McDade, S.S., Henry, A.E., Pivato, G.P., Kozarewa, I., Mitsopoulos, C., Fenwick, K., Assiotis, I., Hakas, J., Zvelebil, M., Orr, N. *et al.* (2012) Genome-wide analysis of p63 binding sites identifies AP-2 factors as co-regulators of epidermal differentiation. *Nucleic Acids Res.*, **40**, 7190–7206.
11. Fakhouri, W.D., Rhea, L., Du, T., Sweezer, E., Morrison, H., Fitzpatrick, D., Yang, B., Dunnwald, M. and Schutte, B.C. (2012) MCS9.7 enhancer activity is highly, but not completely, associated with expression of Irf6 and p63. *Dev. Dyn.*, **241**, 340–349.
12. Rahimov, F., Marazita, M.L., Visel, A., Cooper, M.E., Hitchler, M.J., Rubini, M., Domann, F.E., Govil, M., Christensen, K., Bille, C. *et al.* (2008) Disruption of an AP-2alpha binding site in an IRF6 enhancer is associated with cleft lip. *Nat. Genet.*, **40**, 1341–1347.
13. Kousa, Y.A., Fuller, E. and Schutte, B.C. (2018) IRF6 and AP2A interaction regulates epidermal development. *J. Invest. Dermatol.*, **138**, 2578–2588.
14. Botti, E., Spallone, G., Moretti, F., Marinari, B., Pinetti, V., Galanti, S., De Meo, P.D., De Nicola, F., Ganci, F., Castrignano, T. *et al.* (2011) Developmental factor IRF6 exhibits tumor suppressor activity in squamous cell carcinomas. *Proc. Natl. Acad. Sci. U. S. A.*, **108**, 13710–13715.
15. de la Garza, G., Schleiffarth, J.R., Dunnwald, M., Mankad, A., Weirather, J.L., Bonde, G., Butcher, S., Mansour, T.A., Kousa, Y.A., Fukazawa, C.F. *et al.* (2012) Interferon regulatory factor 6 promotes differentiation of the periderm by activating expression of Grainyhead-like 3. *J. Invest. Dermatol.*, **133**, 68–77.

16. Ting, S.B., Wilanowski, T., Auden, A., Hall, M., Voss, A.K., Thomas, T., Parekh, V., Cunningham, J.M. and Jane, S.M. (2003) Inositol- and folate-resistant neural tube defects in mice lacking the epithelial-specific factor Grhl-3. *Nat. Med.*, **9**, 1513–1519.
17. Smith, A.L., Kousa, Y.A., Kinoshita, A., Fodor, K., Yang, B. and Schutte, B.C. (2017) Generation and characterization of a conditional allele of Interferon Regulatory Factor 6. *Genesis*, **55**. doi: 10.1002/dvg.23038.
18. Blackburn, J., Ohazama, A., Kawasaki, K., Otsuka-Tanaka, Y., Liu, B., Honda, K., Rountree, R.B., Hu, Y., Kawasaki, M., Birchmeier, W. *et al.* (2012) The role of Irf6 in tooth epithelial invagination. *Dev. Biol.*, **365**, 61–70.
19. Iwata, J., Suzuki, A., Pelikan, R.C., Ho, T.V., Sanchez-Lara, P.A., Urata, M., Dixon, M.J. and Chai, Y. (2013) Smad4-Irf6 genetic interaction and TGFbeta-mediated IRF6 signaling cascade are crucial for palatal fusion in mice. *Development*, **140**, 1220–1230.
20. Brewer, S., Jiang, X., Donaldson, S., Williams, T. and Sucov, H.M. (2002) Requirement for AP-2alpha in cardiac outflow tract morphogenesis. *Mech. Dev.*, **110**, 139–149.
21. Kohlbecker, A., Lee, A.E. and Schorle, H. (2002) Exencephaly in a subset of animals heterozygous for AP-2alpha mutation. *Teratology*, **65**, 213–218.
22. Martin, D.I. and Whitelaw, E. (1996) The vagaries of variegating transgenes. *Bioessays*, **18**, 919–923.
23. Reid, B.S., Yang, H., Melvin, V.S., Taketo, M.M. and Williams, T. (2011) Ectodermal Wnt/beta-catenin signaling shapes the mouse face. *Dev. Biol.*, **349**, 261–269.
24. Nelson, D.K. and Williams, T. (2004) Frontonasal process-specific disruption of AP-2alpha results in postnatal midfacial hypoplasia, vascular anomalies, and nasal cavity defects. *Dev. Biol.*, **267**, 72–92.
25. Copp, A.J., Greene, N.D. and Murdoch, J.N. (2003) The genetic basis of mammalian neurulation. *Nat. Rev. Genet.*, **4**, 784–793.
26. Froster-Iskenius, U.G. (1990) Popliteal pterygium syndrome. *J. Med. Genet.*, **27**, 320–326.
27. Escobar, V. and Weaver, D. (1978) Popliteal pterygium syndrome: a phenotypic and genetic analysis. *J. Med. Genet.*, **15**, 35–42.
28. Liu, J.P. and Jessell, T.M. (1998) A role for rhoB in the delamination of neural crest cells from the dorsal neural tube. *Development*, **125**, 5055–5067.
29. Soldano, K.L., Garrett, M.E., Cope, H.L., Rusnak, J.M., Ellis, N.J., Dunlap, K.L., Speer, M.C., Gregory, S.G. and Ashley-Koch, A.E. (2013) Genetic association analyses of nitric oxide synthase genes and neural tube defects vary by phenotype. *Birth Defects Res. B Dev. Reprod. Toxicol.*, **98**, 365–373.
30. Lei, Y., Zhu, H., Yang, W., Ross, M.E., Shaw, G.M. and Finnell, R.H. (2014) Identification of novel CELSR1 mutations in spina bifida. *PLoS One*, **9**, e92207, 10.
31. Kibar, Z., Bosoi, C.M., Kooistra, M., Salem, S., Finnell, R.H., De Marco, P., Merello, E., Bassuk, A.G., Capra, V. and Gros, P. (2009) Novel mutations in VANGL1 in neural tube defects. *Hum. Mutat.*, **30**, E706–E715.
32. Zhang, M.Q. (1998) Statistical features of human exons and their flanking regions. *Hum. Mol. Genet.*, **7**, 919–932.
33. Chen, W., Lam, S.S., Srinath, H., Jiang, Z., Correia, J.J., Schiffer, C.A., Fitzgerald, K.A., Lin, K. and Royer, W.E. Jr. (2008) Insights into interferon regulatory factor activation from the crystal structure of dimeric IRF5. *Nat. Struct. Mol. Biol.*, **15**, 1213–1220.
34. Li, E.B., Truong, D., Hallett, S.A., Mukherjee, K., Schutte, B.C. and Liao, E.C. (2017) Rapid functional analysis of computationally complex rare human IRF6 gene variants using a novel zebrafish model. *PLoS Genet.*, **13**, e1007009 10.
35. Knight, A.S., Schutte, B.C., Jiang, R. and Dixon, M.J. (2006) Developmental expression analysis of the mouse and chick orthologues of IRF6: the gene mutated in Van der Woude syndrome. *Dev. Dyn.*, **235**, 1441–1447.
36. Zucchero, T.M., Cooper, M.E., Maher, B.S., Daack-Hirsch, S., Nepomuceno, B., Ribeiro, L., Caprau, D., Christensen, K., Suzuki, Y., Machida, J. *et al.* (2004) Interferon regulatory factor 6 (IRF6) gene variants and the risk of isolated cleft lip or palate. *N. Engl. J. Med.*, **351**, 769–780.
37. Leslie, E.J., Standley, J., Compton, J., Bale, S., Schutte, B.C. and Murray, J.C. (2012) Comparative analysis of IRF6 variants in families with Van der Woude syndrome and popliteal pterygium syndrome using public whole-exome databases. *Genet. Med.*, **15**, 338–344.
38. Lemay, P., Guyot, M.C., Tremblay, E., Dionne-Laporte, A., Spiegelman, D., Henrion, E., Diallo, O., De Marco, P., Merello, E., Massicotte, C. *et al.* (2015) Loss-of-function de novo mutations play an important role in severe human neural tube defects. *J. Med. Genet.*, **52**, 493–497.
39. Agopian, A.J., Bhalla, A.D., Boerwinkle, E., Finnell, R.H., Grove, M.L., Hixson, J.E., Shimmin, L.C., Sewda, A., Stuart, C., Zhong, Y. *et al.* (2013) Exon sequencing of PAX3 and T (brachyury) in cases with spina bifida. *Birth Defects Res. A Clin. Mol. Teratol.*, **97**, 597–601.
40. Anbanandam, A., Albarado, D.C., Nguyen, C.T., Halder, G., Gao, X. and Veeraraghavan, S. (2006) Insights into transcription enhancer factor 1 (TEF-1) activity from the solution structure of the TEA domain. *Proc. Natl. Acad. Sci. U. S. A.*, **103**, 17225–17230.
41. Zhao, B., Ye, X., Yu, J., Li, L., Li, W., Li, S., Lin, J.D., Wang, C.Y., Chinnaiyan, A.M., Lai, Z.C. *et al.* (2008) TEAD mediates YAP-dependent gene induction and growth control. *Genes Dev.*, **22**, 1962–1971.
42. Cao, X., Pfaff, S.L. and Gage, F.H. (2008) YAP regulates neural progenitor cell number via the TEA domain transcription factor. *Genes Dev.*, **22**, 3320–3334.
43. Sarris, C.E., Tomei, K.L., Carmel, P.W. and Gandhi, C.D. (2012) Lipomyelomeningocele: pathology, treatment, and outcomes. *Neurosurg. Focus*, **33**, E3 10.
44. Goudy, S., Angel, P., Jacobs, B., Hill, C., Mainini, V., Smith, A.L., Kousa, Y.A., Caprioli, R., Prince, L.S., Baldwin, S. *et al.* (2013) Cell-autonomous and non-cell-autonomous roles for IRF6 during development of the tongue. *PLoS One*, **8**, e56270 10.
45. Gustavsson, P., Greene, N.D., Lad, D., Pauws, E., de Castro, S.C., Stanier, P. and Copp, A.J. (2007) Increased expression of grainyhead-like-3 rescues spina bifida in a folate-resistant mouse model. *Hum. Mol. Genet.*, **16**, 2640–2646.
46. Feng, W., Huang, J., Zhang, J. and Williams, T. (2008) Identification and analysis of a conserved Tcfap2a intronic enhancer element required for expression in facial and limb bud mesenchyme. *Mol. Cell Biol.*, **28**, 315–325.
47. Byrne, C., Tainsky, M. and Fuchs, E. (1994) Programming gene expression in developing epidermis. *Development*, **120**, 2369–2383.
48. Fantauzzo, K.A. and Soriano, P. (2014) PI3K-mediated PDGFRalpha signaling regulates survival and proliferation in skeletal development through p53-dependent intracellular pathways. *Genes Dev.*, **28**, 1005–1017.
49. Wilson, N.R., Olm-Shipman, A.J., Acevedo, D.S., Palaniyandi, K., Hall, E.G., Kosa, E., Stumpff, K.M., Smith, G.J., Pitstick,

L., Liao, E.C. *et al.* (2016) SPECC1L deficiency results in increased adherens junction stability and reduced cranial neural crest cell delamination. *Sci. Rep.*, **6**, 17735.
50. Pyrgaki, C., Liu, A. and Niswander, L. (2011) Grainyhead-like 2 regulates neural tube closure and adhesion molecule expression during neural fold fusion. *Dev. Biol.*, **353**, 38–49.
51. Takeda, K., Takeuchi, O., Tsujimura, T., Itami, S., Adachi, O., Kawai, T., Sanjo, H., Yoshikawa, K., Terada, N. and Akira, S. (1999) Limb and skin abnormalities in mice lacking IKKalpha. *Science*, **284**, 313–316.
52. Holland, P., Willis, C., Kanaly, S., Glaccum, M., Warren, A., Charrier, K., Murison, J., Derry, J., Virca, G., Bird, T. *et al.* (2002) RIP4 is an ankyrin repeat-containing kinase essential for keratinocyte differentiation. *Curr. Biol.*, **12**, 1424–1428.
53. Lee, S., Kong, Y. and Weatherbee, S.D. (2013) Forward genetics identifies Kdf1/1810019J16Rik as an essential regulator of the proliferation-differentiation decision in epidermal progenitor cells. *Dev. Biol.*, **383**, 201–213.
54. Li, Q., Estepa, G., Memet, S., Israel, A. and Verma, I.M. (2000) Complete lack of NF-kappaB activity in IKK1 and IKK2 double-deficient mice: additional defect in neurulation. *Genes Dev.*, **14**, 1729–1733.
55. Lahtela, J., Nousiainen, H.O., Stefanovic, V., Tallila, J., Viskari, H., Karikoski, R., Gentile, M., Saloranta, C., Varilo, T., Salonen, R. *et al.* (2010) Mutant CHUK and severe fetal encasement malformation. *N. Engl. J. Med.*, **363**, 1631–1637.
56. Kousa, Y.A., Mansour, T.A., Seada, H., Matoo, S. and Schutte, B.C. (2017) Shared molecular networks in orofacial and neural tube development. *Birth Defects Res.*, **109**, 169–179.
57. Christianson, A., Howson, C.P. and Modell, B. (2006) *March of Dimes Birth Defects Foundation*. White Plains, New York.
58. Yu, Z., Lin, K.K., Bhandari, A., Spencer, J.A., Xu, X., Wang, N., Lu, Z., Gill, G.N., Roop, D.R., Wertz, P. *et al.* (2006) The grainyhead-like epithelial transactivator Get-1/Grhl3 regulates epidermal terminal differentiation and interacts functionally with LMO4. *Dev. Biol.*, **299**, 122–136.
59. Fakhouri, W.D., Rahimov, F., Attanasio, C., Kouwenhoven, E.N., Ferreira De Lima, R.L., Felix, T.M., Nitschke, L., Huver, D., Barrons, J., Kousa, Y.A. *et al.* (2014) An etiologic regulatory mutation in IRF6 with loss- and gain-of-function effects. *Hum. Mol. Genet.*, **23**, 2711–2720.
60. Sharp, T., Wang, J., Li, X., Cao, H., Gao, S., Moreno, M. and Amendt, B.A. (2014) A pituitary homeobox 2 (Pitx2):microRNA-200a-3p:beta-catenin pathway converts mesenchymal cells to amelogenin-expressing dental epithelial cells. *J. Biol. Chem.*, **289**, 27327–27341.
61. de Lima, R.L., Hoper, S.A., Ghassibe, M., Cooper, M.E., Rorick, N.K., Kondo, S., Katz, L., Marazita, M.L., Compton, J., Bale, S. *et al.* (2009) Prevalence and nonrandom distribution of exonic mutations in interferon regulatory factor 6 in 307 families with Van der Woude syndrome and 37 families with popliteal pterygium syndrome. *Genet. Med.*, **11**, 241–247.
62. Howey, R. and Cordell, H.J. (2012) PREMIM and EMIM: tools for estimation of maternal, imprinting and interaction effects using multinomial modelling. *BMC Bioinformatics*, **13**, 149.
63. Qiao, Y., Zhu, Y., Sheng, N., Chen, J., Tao, R., Zhu, Q., Zhang, T., Qian, C. and Jing, N. (2012) AP2gamma regulates neural and epidermal development downstream of the BMP pathway at early stages of ectodermal patterning. *Cell Res.*, **22**, 1546–1561.
64. Wang, X., Pasolli, H.A., Williams, T. and Fuchs, E. (2008) AP-2 factors act in concert with Notch to orchestrate terminal differentiation in skin epidermis. *J. Cell Biol.*, **183**, 37–48.